

Efficient Application of Tensor Network Operators to Tensor Network States

Richard M. Milbradt , ^{*} Shuo Sun , [†] Christian B. Mendl , [‡] Johnnie Gray  and Garnet K.-L. Chan 

¹Technical University of Munich, CIT, Department of Computer Science, Boltzmannstraße 3, 85748 Garching, Germany

²Technical University of Munich, Institute for Advanced Study, Lichtenbergstraße 2a, 85748 Garching, Germany

³Division of Chemistry and Chemical Engineering,
California Institute of Technology, Pasadena, CA 91125, USA

(Dated: January 28, 2026)

The performance of tensor network methods has seen constant improvements over the last few years. We add to this effort by introducing a new algorithm that efficiently applies tree tensor network operators to tree tensor network states inspired by the density matrix method and the Cholesky decomposition. This application procedure is a common subroutine in tensor network methods. We explicitly include the special case of tensor train structures and demonstrate how to extend methods commonly used in this context to general tree structures. We compare our newly developed method with the existing ones in a benchmark scenario with random tensor network states and operators. We find our Cholesky-based compression (CBC) performs equivalently to the current state-of-the-art method, while outperforming most established methods by at least an order of magnitude in runtime. We then apply our knowledge to perform circuit simulation of tree-like circuits, in order to test our method in a more realistic scenario. Here, we find that more complex tree structures can outperform simple linear structures and achieve lower errors than those possible with the simple structures. Additionally, our CBC still performs among the most successful methods, showing less dependence on the different bond dimensions of the operator.

I. INTRODUCTION

Tensor networks have proven to be powerful tools for simulating large quantum systems, including quantum circuit simulation, quantum chemistry, and many-body physics, among others. Here, we will focus on one specific subroutine for tensor network methods, which is the efficient evaluation of

$$\hat{O} |\psi\rangle, \quad (1)$$

where \hat{O} is a quantum operator and $|\psi\rangle$ is a quantum state, and both are given as a tensor network. However, we will restrict ourselves to loop-free tensor networks, so-called tree tensor networks (TTN) [1, 2], which will be introduced in Sec. II in more detail. This special class of tensor network has proven useful in various applications [1, 3–16]. For the special case of linear TTN, known as tensor trains or matrix product states (MPS), there is already a variety of algorithms that evaluate Eq. (1), such as the density matrix-based, Zip-Up, and successive randomized compression algorithms. We will take a closer look at these methods in Sec. III after introducing our new Cholesky decomposition-based algorithm for both tensor trains and general tree structures. The application subroutine itself has been utilized in a diverse range of simulation procedures, including the computation of ground states and other low-lying states [17–21], as well as the approximate contraction of two-dimensional tensor networks [22, 23]. Another common use case is simulating the time evolution of quantum systems. This is

either done by directly representing the time-evolution operator as an appropriate tensor network [24–26] or by utilising this subroutine to perform Krylov-like methods [27–29]. Two special cases of time evolution are the simulation of open quantum systems in the influence functional framework [30–33] and the simulation of quantum circuits [34, 35]. We will use a toy problem with random TTNs and a quantum circuit simulation to compare our new method to the already existing ones in Sec. IV.

II. TREE TENSOR NETWORKS

This chapter introduces the nomenclature used in this work regarding tensor networks. It is assumed that the reader is familiar with the basics of tensor networks, including contractions and decompositions. More pedagogical and in-depth introductions can be found in [2, 36–38]. For a quick overview, consider the recent reviews [39–41].

A. Tree Tensor Network States

Rather than representing a quantum state $|\psi\rangle \in \mathbb{C}^{d_1 \times \dots \times d_L}$ of L sites, where site i has local dimension d_i , as a state vector, we can describe it as a tree tensor network state (TTNS) [1]. Thus, we write the state as

$$|\psi\rangle = \sum_{\vec{\sigma}, \vec{\alpha}} T_{\sigma_1 \vec{\alpha}_1}^{[1]} \cdots T_{\sigma_L \vec{\alpha}_L}^{[L]} |\sigma_1 \cdots \sigma_L\rangle, \quad (2)$$

where $\{|\sigma_i\rangle\}_{\sigma_i=1}^{d_i}$ is the local basis of site i , where d_i can be 1. The vector $\vec{\alpha}_i$ contains all virtual legs of $T^{[i]}$, the leg contracted with the parent site of i will always be $\alpha_{i,0}$.

^{*} r.milbradt@tum.de

[†] shuo.sun@in.tum.de

[‡] christian.mendl@tum.de

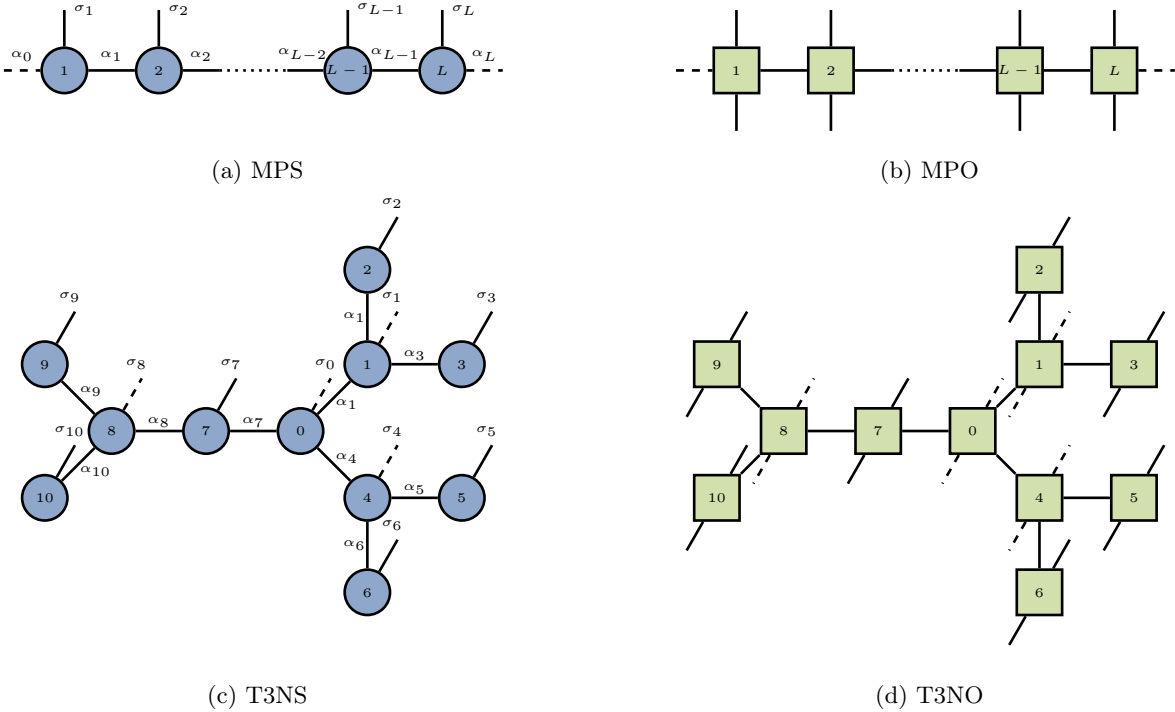


FIG. 1: Diagrammatic representation of the different tree tensor networks. The dashed lines denote a trivial leg, i.e., one of dimension 1. The upper two tensor networks are tensor-trains, while the lower two are T3NS. The two TTNS on the left represent quantum states, i.e., they are TTNS, while the two on the right represent quantum operators, i.e., TTNOs. The labels on the latter's legs were omitted for visual clarity.

Additionally, the leg α_i is the virtual leg of the site tensor $T^{[i]}$ that is contracted with the tensor of the parent site of i while the vector $\vec{\alpha}_i$ contains all the virtual legs that are contracted with a tensor of a child site of i . The parent-child relationship between nodes defines a hierarchy, thereby establishing a tree structure. We will denote the set of children of site i as C_i and the parent as p_i , as it is usually clear from the context which site is intended. Note that our definition of a tree structure is a rooted tree and implies that there is one site r without a parent called the root. For it, the parent leg α_r is of dimension 1 to make Eq. (2) consistent. However, in our context, this choice is arbitrary and merely used for an easier description of the following algorithms. It is trivial to extend all of them to non-rooted trees. Finally, note that we do not make a clear distinction between a given leg of a tensor and its index values in a contraction sum to simplify the required notation. We will now examine a few special TTNS used throughout this work.

B. Special Tree Structures

The matrix product state (MPS) [36], also known as tensor train [42], is the most commonly used tensor network to represent a quantum state. It is a chain of tensors with two virtual and one physical leg each, where the one virtual leg of the first and last tensor is trivial. This

structure can be viewed as a TTNS, where every site has at most one child. We will use a slightly different notation compared to Eq. (2) and represent a quantum state $|\psi\rangle \in \mathbb{C}^{d_1 \times \dots \times d_L}$ of L sites by

$$|\psi\rangle = \sum_{\sigma, \vec{\alpha}} T_{\sigma_1 \alpha_0 \alpha_1}^{[1]} \dots T_{\sigma_L \alpha_{L-1} \alpha_L}^{[L]} |\sigma_1 \dots \sigma_L\rangle \quad (3)$$

where the outermost legs α_0 and α_L are of dimension 1. Note that we changed the notation for the virtual legs: The leg to the left and right of site i are denoted α_{i-1} and α_i respectively. Since it has been so widely used in research over the last two decades, one cannot hope to state all its use cases. Examples include condensed matter physics, quantum information, open quantum systems, and quantum chemistry. A graphical depiction of the MPS structure is given in Fig. 1a. Note that in this work, we will refer to the underlying structure as the tensor train structure, but when used to represent a quantum state, we will refer to the state as an MPS.

The second important tree structure is the T3NSs. A T3NS is a tree tensor network state for which no node has more than three non-trivial legs [43]. Notably, this means that only a site with a maximum of two non-trivial virtual legs can also have a non-trivial physical leg. This limitation of legs tends to leave the scaling of algorithms acceptable while still allowing for the full flexibility in creating topologically adapted tree tensor network structures. However, especially in cases where physical dimen-

sions are small, it can sometimes be advisable to allow multiple open legs per tensor, while still restricting the number of virtual legs, which tend to have a much higher dimension [9, 10, 44–46]. Thus, T3NS have mainly been used in quantum chemistry [13, 14, 16, 43, 47] or in a setting with mostly non-physical sites neighboring each other [8, 48–52]. An example of a T3NS is depicted in Fig. 1c.

These are the two main tree structures needed for now. We will explain additional structures as needed, though we will mostly refrain from drawing the leg indices into the tensor network diagrams to avoid unnecessary clutter.

C. Tree Tensor Network Operators

Another kind of tensor network, essential for this work, is the tree tensor network operator (TTNO) [53, 54]. Analogously to TTNS representing quantum states, TTNOs represent linear operators acting on a quantum state. Thus a linear operator $\hat{O} : \mathbb{C}^{\times d_i} \rightarrow \mathbb{C}^{\times d_i}$ acting on a multi-site quantum system can be written as

$$\hat{O} = \sum_{\vec{\sigma}', \vec{\sigma}, \vec{\beta}} \mathcal{T}_{\sigma'_1 \sigma_1 \beta_1}^{[1]} \cdots \mathcal{T}_{\sigma'_L \sigma_L \beta_L}^{[L]} \cdot |\sigma'_1 \cdots \sigma'_L \rangle \langle \sigma_1 \cdots \sigma_L|. \quad (4)$$

This resembles the definition of the TTNS in Eq. (2), apart from the additional physical leg on each tensor. We will also use the same notation for the legs and indices of TTNO tensors as well as the special notation for the tensor train equivalent of the TTNO, the matrix product operator (MPO). Both an MPO and a T3NO, i.e., the operator equivalent of a T3NS, are depicted in Fig. 1b and Fig. 1d, respectively. Use cases for a TTNO are ground state search [7, 11] and time-evolution algorithms [50, 52, 55–57]. In these algorithms, the TTNO represents the system's Hamiltonian, which can be constructed efficiently for arbitrary tree structures [54, 58, 59]. However, most of these algorithms merely require something akin to the expectation value $\langle \psi | \hat{O} | \psi \rangle$ and not the state $|\psi'\rangle = \hat{O}|\psi\rangle$ resulting from the application of \hat{O} to $|\psi\rangle$. Algorithms requiring this are currently rarely used with TTN, cf. [16] for an example. However, the algorithms that require the application of MPO to MPS, as highlighted in I, are easily generalizable to TTN. Thus, we will now show how to obtain $|\psi'\rangle$ for tensor trains and more general tree structures.

III. CHOLESKY BASED COMPRESSION

We will now state the general idea for our new compression algorithm, coined the Cholesky Based Compression (CBC). A step-by-step description can be found in Sec. IIIA and Sec. IIIB for tensor-trains and general TTN, respectively. The general idea is based on the fact

that any TTNS is split into two disconnected subsystems A and B by cutting any virtual bond α_i . The required dimension of this bond can then be obtained by performing the eigendecomposition of the resulting density matrix, which is obtained by performing the partial trace over all sites connected to site i only via leg α_i . To avoid exponential scaling, the physical degrees of freedom for which the tensor was already compressed are removed through a projection, compressing them into a single virtual degree of freedom. In the end, one obtains the new and compressed TTNS as a projection change of the original TTNS into the compressed form. This idea is known as the density matrix compression algorithm (DMC). It was originally introduced for MPS only [60], but a version for general TTNS was recently introduced [61]. However, when constructing the tensor representing the reduced density matrix, we build many local positive definite tensors explicitly by evaluating a product of the form $G = M^\dagger M$, which is a Cholesky decomposition of G . In the CBC, we utilize this fact by constructing only M and immediately truncating the legs that would connect to the adjoint. Avoiding the full construction of the tensor G leads to a more efficient algorithm as the involved tensors tend to be much smaller, as we will see in the explicit statement of the algorithm.

A. Tensor Train Structure

For the chain-like tensor train structure, start from the leftmost site and obtain a left environment, similar to that in DMRG, for every site. To do so, we start performing the contraction

$$\mathcal{L}'^{[i]}_{\chi_{i-1} \sigma' \alpha_i \beta_i} = \sum_{\substack{\sigma_i \\ \alpha_{i-1} \beta_{i-1}}} \mathcal{L}^{[i-1]}_{\chi_{i-1} \alpha_{i-1} \beta_{i-1}} \mathcal{T}_{\sigma'_i \sigma_i \beta_{i-1} \beta_i}^{[i]} T_{\sigma_i \alpha_i \alpha_{i-1}}^{[i]} \quad (5)$$

for site i with $\mathcal{L}^{[0]} = 1$ as a initial condition. As a next step we combine the χ_{i-1} and σ' legs of $\mathcal{L}'^{[i]}$ into one leg (χ_{i-1}, σ') . The newly obtained leg (χ_{i-1}, σ') is then compressed down to the desired new bond dimension \bar{D} , for example via singular value decomposition. This yields the new leg χ_i and the tensor $\mathcal{L}^{[i]}$, which is saved for later. Any isometric tensor on the other end of leg χ_i , i.e., a tensor that now has the large leg (χ_{i-1}, σ') , can be dropped as it would be canceled in the later steps anyways. A diagrammatic version of this procedure is shown in Fig. 2a. We do this for all sites except the rightmost one, $i = L$, for which no action is needed in this sweep.

Once we reach the rightmost site, we perform a sweep backwards with the following steps for each site. We

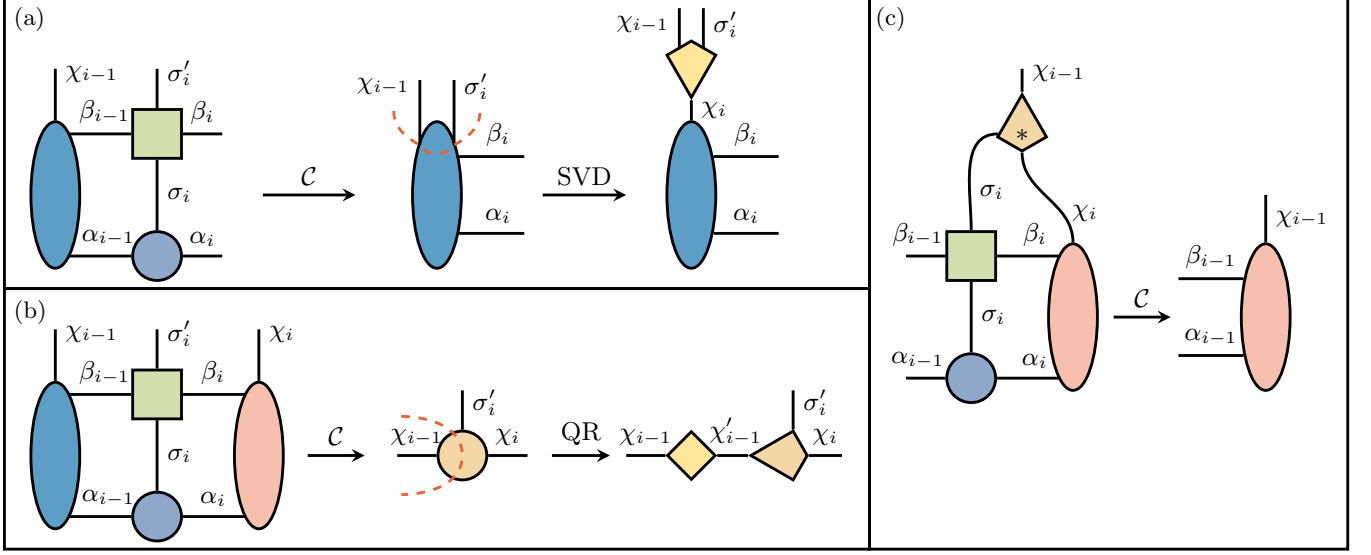


FIG. 2: The different steps of the CBC for a tensor train structure. a) The contraction Eq. (5) and subsequent truncation, b) the contraction Eq. (6) and subsequent QR-decomposition Eq. (7) to obtain the new local tensor, c) the final contraction Eq. (8) to find the new projected subsystem tensor used for the next site. Note that the yellow tensors are not used in later steps and can be deleted.

perform the contraction

$$\mathcal{S}_{\sigma'_i \chi_{i-1} \chi_i}^{[i]} = \sum_{\substack{\sigma \\ \alpha_{i-1} \beta_{i-1} \\ \alpha_i \beta_i}} \mathcal{L}_{\chi_{i-1} \alpha_{i-1} \beta_{i-1}}^{[i-1]} \mathcal{T}_{\sigma'_i \sigma_i \beta_i \beta_{i-1}}^{[i]} \cdot T_{\sigma_i \alpha_i \alpha_{i-1}}^{[i]} \mathcal{R}_{\chi_i \alpha_i \beta_i}^{[i]} \quad (6)$$

with the initial condition $\mathcal{R}^{[L]} = 1$. If we are at the leftmost site $i = 1$, $\mathcal{S}^{[1]}$ will be the new MPS tensor $T'^{[1]}$. Otherwise, we continue and perform a QR-decomposition on leg χ_{i-1} of $\mathcal{S}^{[i]}$ to obtain

$$\mathcal{S}_{\sigma'_i \chi_{i-1} \chi_i}^{[i]} = \sum_{\chi'_{i-1}} R_{\chi_{i-1} \chi'_{i-1}} Q_{\sigma'_i \chi'_{i-1} \chi_i}^{[i]} \quad (7)$$

of which we assign the isometric tensor $Q^{[i]}$ as the new MPS tensor $T'^{[i]}$ of this site. This part of the procedure is shown in Fig. 2b. We then obtain the new tensor $\mathcal{R}^{[i-1]}$ by performing the contraction

$$\mathcal{R}_{\chi'_{i-1} \alpha_{i-1} \beta_{i-1}}^{[i-1]} = \sum_{\substack{\sigma'_i \sigma_i \chi_i \\ \alpha_i \beta_i}} Q_{\sigma'_i \chi'_{i-1} \chi_i}^{[i]*} T_{\sigma_i \alpha_{i-1} \alpha_i}^{[i]} \cdot \mathcal{T}_{\sigma'_i \sigma_i \beta_{i-1} \beta_i}^{[i]} \mathcal{R}_{\chi_i \alpha_i \beta_i}^{[i]}. \quad (8)$$

This contraction is shown graphically in Fig. 2c. Then we continue with the next site. To reiterate, once the leftmost site is reached, we merely perform the contraction in Eq. (6) and we will have obtained our new MPS tensors as

$$T'^{[i]} = \begin{cases} \mathcal{S}^{[i]} & \text{if } i = 0 \\ Q^{[i]} & \text{else.} \end{cases} \quad (9)$$

A detailed run through of this process for an MPS of length 4 is shown in App. Sec. A.

B. Tree Structures

We now extend the CBC algorithm to tensor networks with a tree structure. The graphical depiction of one step for T3NS is shown in Fig. 3. Overall, the algorithm works analogously to the tensor train case. As a first step, we construct the initial tensor blocks. This splits into two slightly different parts. In the first, we move up from the leaves to the root. For each site i , we perform the contraction

$$\mathcal{L}_{\sigma'_i \vec{\chi}_i \setminus 0 \alpha_0 \beta_0}^{[i]} = \sum_{\substack{\sigma_i \\ \vec{\alpha}_i \setminus 0 \\ \vec{\beta}_i \setminus 0}} T_{\sigma_i \vec{\alpha}_i}^{[i]} \mathcal{T}_{\sigma'_i \sigma_i \vec{\beta}_i}^{[i]} \prod_{c \in C_i} \mathcal{L}_{\chi_c \alpha_c \beta_c}^{[c]}. \quad (10)$$

We then join the legs $(\sigma'_i, \vec{\chi}_i)$ into one and compress it as we did in the previous section. This yields the new leg χ_i with desired bond dimension D and the tensor $\mathcal{L}^{[i]}$. These steps are shown in Fig. 3a. Once we reach the root of the tree, we perform the following steps for every site i except the leaves, as we move down the tree. For each $k \in C$ we contract

$$\begin{aligned} \mathcal{L}_{\sigma'_i \vec{\chi}_i \setminus k \alpha_k \beta_k}^{[(i,k)]} = & \sum_{\substack{\sigma_i \\ \vec{\alpha}_i \setminus k \\ \vec{\beta}_i \setminus k}} T_{\sigma_i \vec{\alpha}_i}^{[i]} \mathcal{T}_{\sigma'_i \sigma_i \vec{\beta}_i}^{[i]} \\ & \cdot \mathcal{L}_{\chi_0 \alpha_0 \beta_0}^{[(p,i)]} \prod_{c \in C_i \setminus k} \mathcal{L}_{\chi_c \alpha_c \beta_c}^{[c]}. \end{aligned} \quad (11)$$

We combine the legs $(\sigma'_i, \vec{\chi}_i \setminus k)$ into one and compress it, yielding the leg χ_i and the tensor $\mathcal{L}^{[(i,k)]}$. The three steps are shown in Fig. 3b. These first two parts are almost the same as the steps for the tensor train structure, apart from the choice of which legs are contracted.

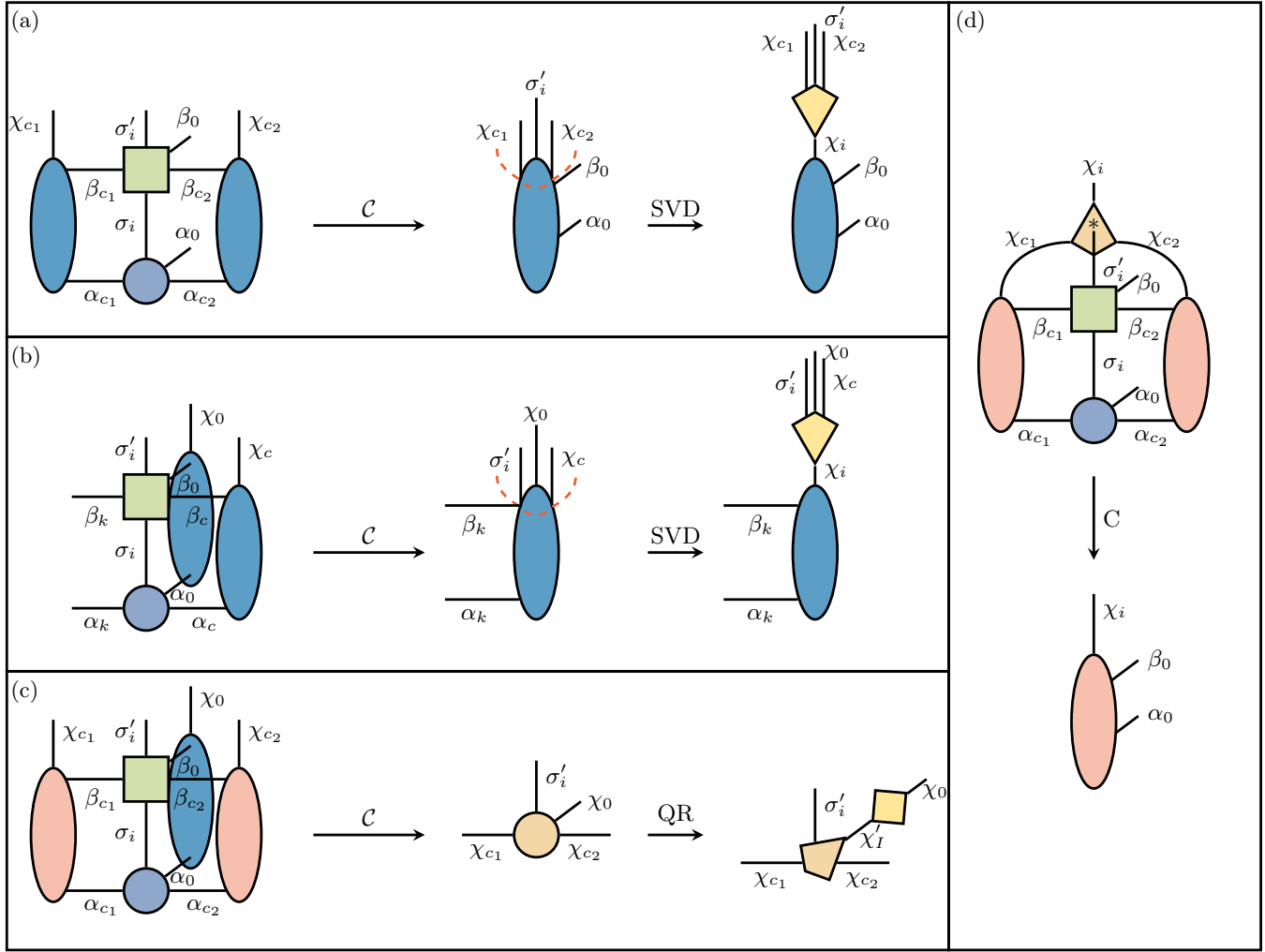


FIG. 3: The different steps of the CBC for a T3NS structure. a) The contraction and truncation from leafs to root Eq. (10), b) the contraction and truncation from the root to the leafs Eq. (11), c) The contraction Eq. (12) and subsequent QR-decomposition Eq. (13) to obtain the new local tensor, d) the final contraction Eq. (14) to obtain the new projected subsystem tensor for the parent site. Note that the yellow tensors are not used in later steps and can be deleted.

Now we do another sweep, starting at the leaf of the tree and moving towards the root. For every site i , we contract

$$\mathcal{S}_{\sigma'_i \vec{\chi}_i} = \sum_{\sigma_i \vec{\alpha}_i \vec{\beta}_i} T_{\sigma_i \vec{\alpha}_i}^{[i]} \mathcal{T}_{\sigma'_i \sigma_i \vec{\beta}_i}^{[i]} \cdot \mathcal{L}_{\chi_0 \alpha_0 \beta_0}^{[(p_i, i)]} \prod_{c \in C_i} \mathcal{R}_{\chi_c \alpha_c \beta_c}^{[c]}, \quad (12)$$

as shown in the first step of Fig. 3c. If i is the root site, we are done and consider $T'^{[i]} = \mathcal{S}^{[i]}$ as the new TTNS tensor. Otherwise we continue by performing a QR decomposition on leg χ_i of $\mathcal{S}^{[i]}$ to obtain

$$\mathcal{S}_{\sigma'_i \vec{\chi}_i}^{[i]} = \sum_{\chi'_i} Q_{\sigma'_i \chi'_i \vec{\chi}_i}^{[i]} R_{\chi'_i \chi_i}. \quad (13)$$

The resulting isometric tensor $Q^{[i]}$ is then assigned to be the new tensor $T'^{[i]}$ in the TTNS. The decomposition is shown as the second step in Fig. 3c. As a final step we obtain the new tensor $\mathcal{R}^{[i]}$ via the contraction

$$\mathcal{R}_{\chi'_0 \alpha_0 \beta_0}^{[i]} = \sum_{\substack{\sigma'_i \sigma_i \\ \vec{\alpha}_i \setminus \vec{\beta}_i \setminus 0 \vec{\chi}_i}} T_{\sigma_i \vec{\alpha}_i}^{[i]} \mathcal{T}_{\sigma'_i \sigma_i \vec{\beta}_i}^{[i]} \cdot Q_{\sigma'_i \chi'_i \vec{\chi}_i}^{[i]} \prod_{c \in C_i} \mathcal{R}_{\chi_c \alpha_c \beta_c}^{[c]}. \quad (14)$$

A graphical depiction of this step is given in Fig. 3d. Then we continue with the parent of this site. So eventually we end up with the new tensors for the TTNS

$$T'^{[i]} = \begin{cases} \mathcal{S}^{[i]} & \text{if } i \text{ is the root} \\ Q^{[i]} & \text{else.} \end{cases} \quad (15)$$

C. Other Compression Methods

We will now provide an overview of other methods commonly used to apply an MPO to an MPS and restrict the resulting bond dimension. Note that, even though for some of these methods, there is no explicit version for general TTN in the literature. However, while not trivial, the method's extension follows a similar scheme to that of the CBC: moving up and down the tree for pre-computation and then performing a second sweep from the leaves to the root. We will also refrain from mentioning the DMC again, as it was already covered at the beginning of this section, c.f. Sec. III.

The simplest way of performing the application and compression is to do both as separate steps. Here, the TTNO is fully contracted with the TTNS, and the two virtual legs between every two nodes are combined into one larger leg. Then the compression is performed as a second step. This compression takes the form of a sweep through the entire network, performing truncated SVDs for each leg encountered during the sweep to compress it down to the desired dimension. The sweep can be performed either from leaves to root, requiring the movement of the orthogonality center [36, 42, 61], or recursively from the root to the leaves with the root as the orthogonality center [52]. The compression can also benefit from using randomized SVD if the difference between the current and desired bond dimension is large [62]. While this approach is the most accurate one [42], it has a worse analytical scaling, also evidenced in numerical benchmarks, compared to the more involved methods [25, 61–63].

The other end of the spectrum is the ZipUp method [64]. It is very fast, but has a small accuracy. The method sweeps through the network only once and compresses every site locally, using the result of already compressed sites. However, the fact that it only utilises the information of the already compressed parts of the tensor network is the cause of the smaller accuracy. The state that is part of this contraction can be brought into canonical form before running the ZipUp method to slightly improve its performance [25]. For a graphical depiction of this method on MPS, consider any of [25, 61, 65].

A recent improved algorithm is the successive randomized compression (SRC) [63]. It utilizes multiple randomly generated tensors to find the compressed product, employing the same underlying ideas as random matrix decompositions [66, 67]. For this algorithm, a single random matrix of size $d \times \bar{D}$ is drawn per site. They are combined via the Khatri-Rao product and contracted to build environment blocks similar to our CBC algorithm. However, instead of an SVD, the compression is obtained through contraction with random matrices. Performance-wise, the obtained state is comparable to that of the naive application and DMC algorithms, while beating the Zip-Up algorithm in runtime [63].

Finally, there is an entire class of algorithms that variationally fit the result to a TTNS of desired bond dimension.

Computational cost	MPS	T3NS
Direct	$\mathcal{O}(Ld^2 D_S^3 D_O^3)$	$\mathcal{O}(Ld^3 D_S^4 D_O^4)$
Density Matrix	$\mathcal{O}(LD_S^2 D_O^2 \bar{D})$	$\mathcal{O}(Ld^3 \bar{D}^6)$
Zip-Up	$\mathcal{O}(Ld D_S D_O \bar{D}^2)$	$\mathcal{O}(Ld D_S D_O \bar{D}^3)$
SRC	$\mathcal{O}(Ld D_S D_O \bar{D}^2)$	$\mathcal{O}(Ld D_S D_O \bar{D}^3)$
CBC	$\mathcal{O}(Ld D_S D_O \bar{D}^2)$	$\mathcal{O}(Ld D_S D_O \bar{D}^3)$

TABLE I: The scaling of the operation count of the different application methods for MPSs and T3NSs under the assumptions $d \leq D_S \leq D_O \leq \bar{D} < D_S D_O$, where d is the maximum physical dimension, D_S and D_O the maximum virtual bond dimension of the state and operator, respectively, and \bar{D} the desired bond dimension after the contraction. Refer to [63] for more general scalings of the MPS methods. The T3NS scalings become too complicated under more general assumptions to be of practical use.

Memory cost	MPS	T3NS
Direct	$\mathcal{O}(d D_S^2 D_O^2)$	$\mathcal{O}(d D_O^3 D_S^3)$
Density Matrix	$\mathcal{O}(d D_O^2 D_S^2)$	$\mathcal{O}(d D_O^4 D_S^4)$
Zip-Up	$\mathcal{O}(d D_O^2 \bar{D}^2)$	$\mathcal{O}(d D_O^3 \bar{D}^3)$
SRC	$\mathcal{O}(d D_O^2 \bar{D}^2)$	$\mathcal{O}(d D_O^3 \bar{D}^3)$
CBC	$\mathcal{O}(d D_O^2 \bar{D}^2)$	$\mathcal{O}(d D_O^3 \bar{D}^3)$

TABLE II: The scaling of memory requirements for the different application methods for MPSs and T3NSs under the assumptions $d \leq D_S \leq D_O \leq \bar{D} < D_S D_O$.

sion. This can be done by first contracting and then performing the fitting, using the contraction result as a reference [25, 36]. A way to perform the application without the explicit contraction can be achieved via DMRG-like sweeps [22, 64]. However, these variational approaches can take a long time to converge or get stuck in local minima without an educated starting guess, for example, obtained via a Zip-Up run [25, 63]. Therefore, we will exclude it from the following numerical exploration.

A simplified scaling of the operation count is presented in Tab. I, and a simplified scaling for the required memory in Tab. II. It highlights that Zip-Up, SRC, and our new CBC have a similar scaling in the required resources. Additionally, we observe that the DM-based algorithm loses some of its advantage over the direct method when going from MPS to the more complex T3NS. We note that this behavior persists for trees with higher degrees, and, in particular, the memory requirements can already become problematic for the T3NS case.

IV. NUMERICAL RESULTS

We will now compare our newly introduced CBC to the other application methods. The numerical simulations were performed using PyTreeNet [68, 69] on an Intel i7-10700 CPU with 32 GB of RAM.

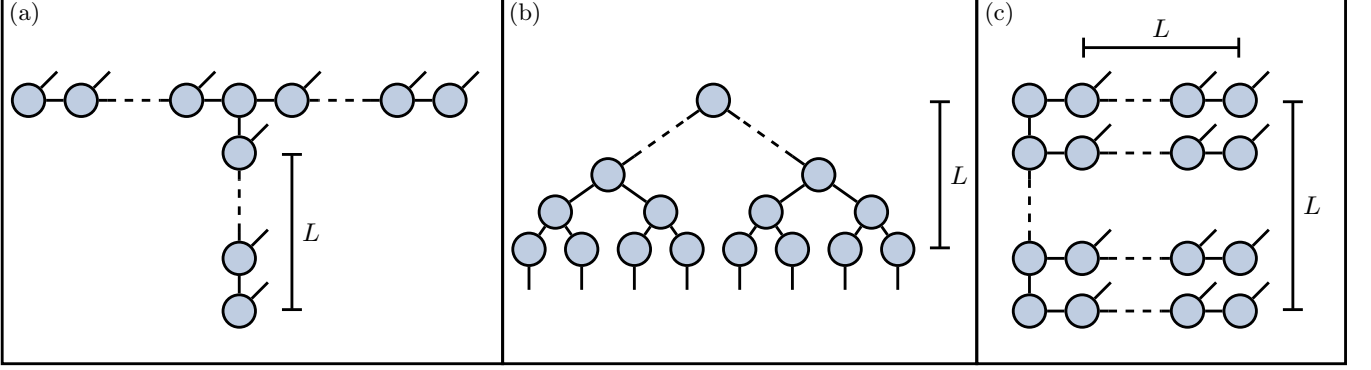


FIG. 4: The three additional tree structures explored in Sec. IV A. a) T-Tree structure, b) binary tree structure, c) the fork tensor product structure. Here, only the TTNSs are depicted. The respective TTNOs have the exact same structure but with two physical legs per node.

A. Random States and Operators

As a first comparison of the methods, we applied random TTNOs to random TTNSs for varying desired bond dimensions. Inspired by [63], both the real and imaginary parts of every element of the TTNOs and the TTNSs were drawn independently from a uniform random distribution on the interval $[-0.5, 1]$. This choice is motivated by the fact that tensor network contraction becomes easier if the tensor elements have a positive bias [63, 70]. We conducted this experiment with four different types of trees. The first one is the tensor train structure with 50 sites and an initial bond dimension of $D_S = D_O = 40$ for both the MPS and the MPO and local dimension $d = 3$. The bond dimension of the exactly contracted tensor networks is $40^2 = 1600$, though we only run our approximation methods until a maximum target bond dimension $\bar{D} = 40$, so equal to the initial bond dimension.

The other three are T3NS with a more restricted structure:

- The *T-Tree* structure, named due to its resemblance to the letter T. There is one central node connected to three chains of nodes with one physical leg each. In general, all three chains can have a different number of nodes each. However, we restrict our exploration to T-trees with the same length L in each chain, allowing us to use this length as the defining system size parameter. A T-tree is depicted in Fig. 4a. As a system size, we use $L = 20$.
- The *binary tree* structure. There is a predefined root node, and every node has at most two children. Additionally, only the leaf nodes are allowed to have physical legs. This is one of the more commonly used tree tensor networks and is sometimes referred to as the tree tensor network [39]. In our numerical experiment, we further restrict this structure by using only perfectly balanced binary trees. That

is, every non-leaf node has exactly two children. Thus, we can use the tree's depth L as the defining system size parameter. A binary TTNS is depicted in Fig. 4b. As a system size, we use $L = 6$.

- The fork tensor product (FTP) structure [71]. The FTP is a rectangular structure with one chain of virtual nodes that do not have a physical leg. Attached to each of these nodes is a chain of nodes with a physical leg. Again, we restrict this structure further, demanding that every chain has the same length L and that the number of virtual nodes is equal to this chain length. Thus, we can use L as the system size parameter defining a square shape. An FTPS is depicted in Fig. 4c. As a system size, we use $L = 8$.

For all three structures, we can only run the exact contraction to a bond dimension of $D_S = D_O = 10$, leading to a resulting bond dimension of $10^2 = 100$, but again with a local dimension $d = 3$. This is due to the significantly higher memory requirement of the tensors with three virtual bonds.

The results of the compressions are collected in Fig. 5. We can see that in both cases, the CBC and SRC perform almost identically and significantly better than the other methods. They outperform the Zip-Up method in both accuracy and, most of the time, also in runtime for a given bond dimension. For a desired error threshold, they outperform the Zip-Up method both in runtime and the required bond dimension. They also outperform the DM and direct methods in runtime by around one order of magnitude for a given error threshold, though the error is slightly worse for a given bond dimension. Comparing the different tree structures, we find that there is a major difference when making the jump from MPS to general T3NS structures. While the different initial bond dimension makes direct performance comparisons difficult, we can clearly see that the DM compression method suddenly performs significantly worse. This is

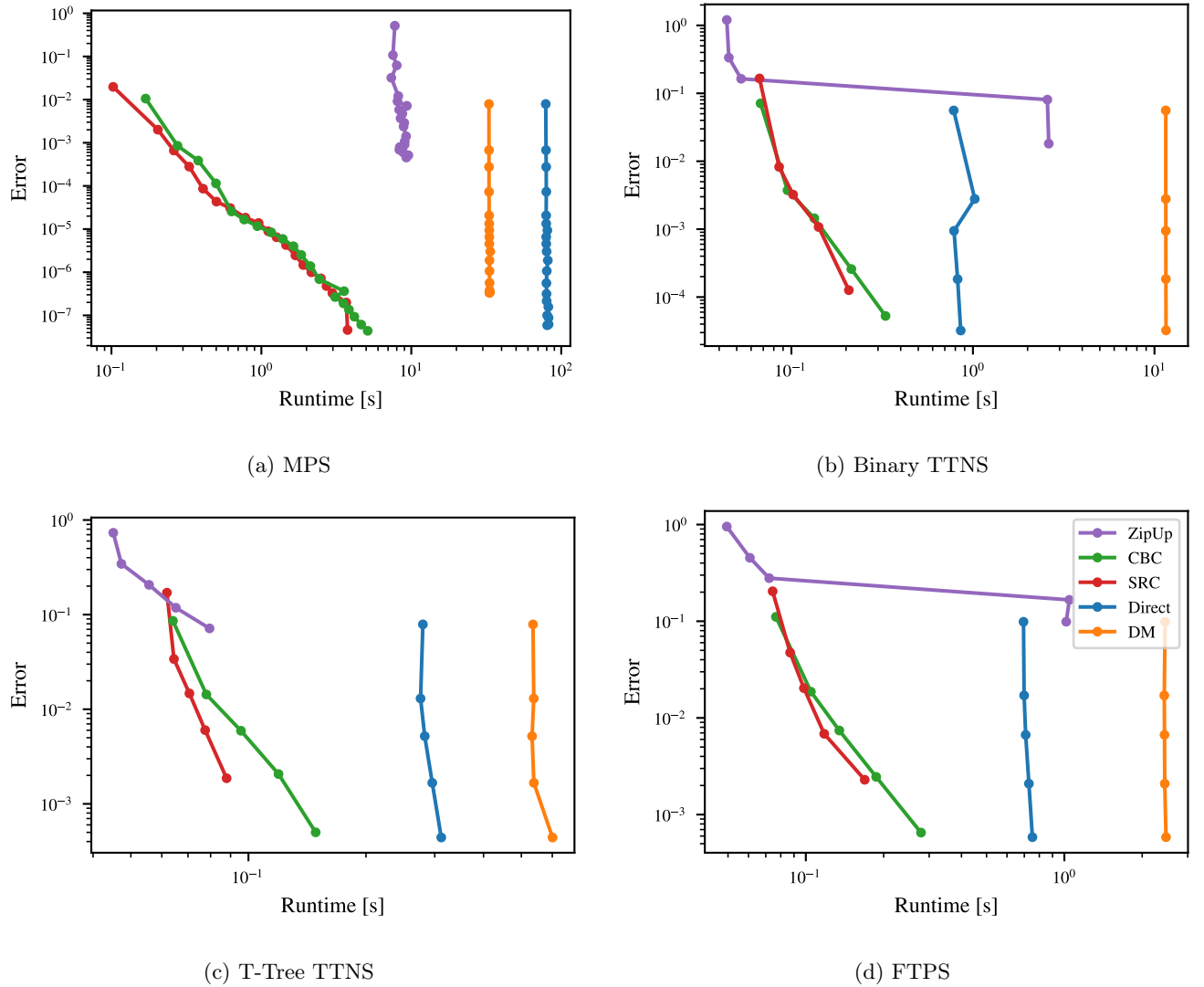


FIG. 5: Error versus runtime plots for the different tree structures, the results for our CBC method are shown in green. Each data point on a line corresponds to the results for one target bond dimension. In the case of the MPS, the bond dimensions range from 2 to 40, while for the other structures, they range from 2 to 10, increasing by 2 with each consecutive data point in both cases.

due to the significantly worse scaling compared to the other methods, as soon as a tensor with three virtual bonds is encountered, cf. Tab. I and Tab. II. Similarly, the runtime difference of the other methods gets closer to the direct method. Since the memory issues do not allow decent comparison between the MPS and T3NS methods, we now look at another benchmark.

B. Circuit Simulation

As a second experiment, we conduct a more realistic simulation that is closer to an actual application by simulating a quantum circuit U_{full} . To avoid the need for a reference calculation, we consider a quantum circuit of

the form

$$U_{\text{full}} = UU^{\dagger}. \quad (16)$$

Accordingly, the output state should be equal to the input state for an exact circuit simulation. The circuit U itself consists of N batches

$$U = \prod_{i=1}^N U_i, \quad (17)$$

each batch U_i has the form shown in Fig. 6 and is thus a tree-like circuit [9]. In the circuit, every two-qubit gate G is of the form

$$G = \text{CNOT} \cdot (V_1 \otimes V_2), \quad (18)$$

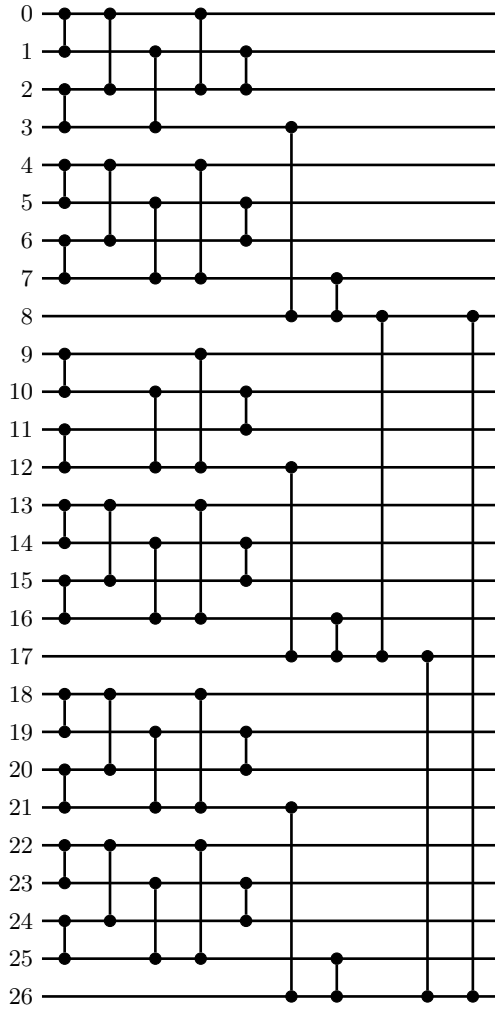


FIG. 6: The structure of one batch of the quantum circuit. Two vertically connected dots represent a two-qubit gate.

where all the single qubit gates V_i are drawn Haar randomly. Note that the V_i are only placed in front of the CNOT, as they do not have any entangling power. Thus, multiple V_i gates applied one after another do not impact the performance of the tensor network method compared to a single such gate. We construct every level of the circuit as shown in Fig. 6 as a separate TTNO, via the method introduced in [59]. The resulting TTNO is then applied to the current TTNS. We run this experiment on three different tree structures. The first is a simple 27-site MPS that is agnostic to the circuit's structure. The other two structures are more complex trees adapted specifically to the entangling structure of the batches U_i . Both structures are T3NS, but one has the highly entangled gates combined into MPS-like structures, shown in Fig. 7a. In the other T3NS, only leaf nodes have physical legs.

We ran this simulation for all tree structures with $N = 3$ layers and bond dimensions \bar{D} ranging from 10 to 200.

The quantum system starts in the computational all-zero state $|\psi_0\rangle = |0\rangle$, and we record the error when comparing the final to the initial state

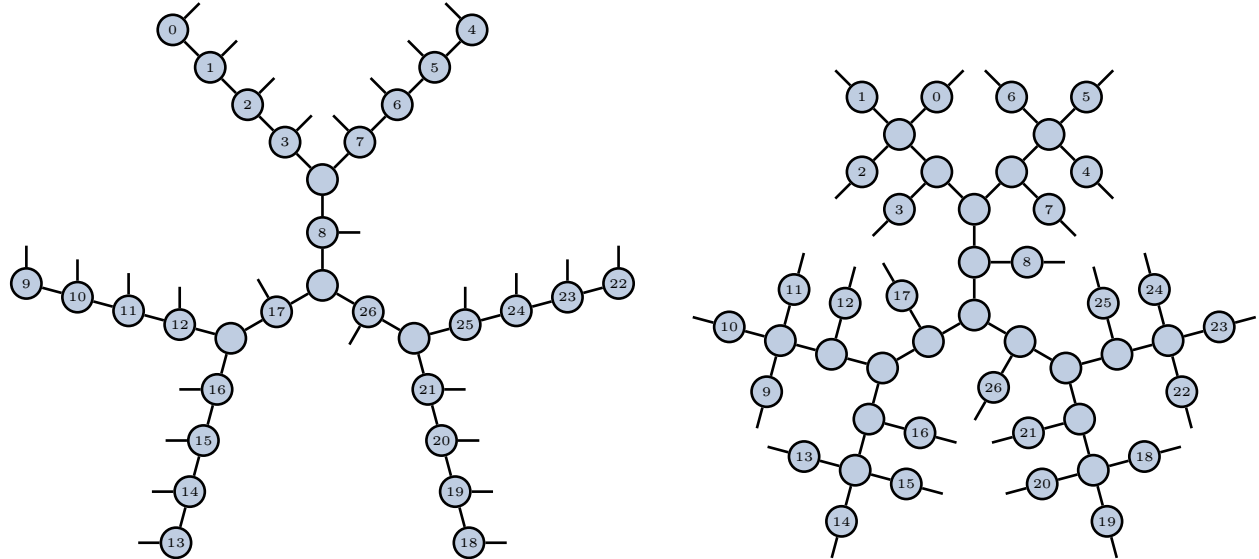
$$\text{Err} = \|\psi_0\rangle - U_{\text{full}}|\psi_0\rangle\|. \quad (19)$$

To compare the performance of the different methods, we not only recorded the runtime but also the maximum size, i.e., the maximum number of tensor entries in the TTNS, during runtime, as a measure of memory requirement. The results averaged over five runs with different seeds for the random gates are plotted in Fig. 8.

The first thing to note is that the Zip-Up method fails to converge to an error much below 1 for any of the three structures, even for the largest bond dimensions. However, the other methods converge to numerical error for a bond dimension of $\bar{D} = 50$ for both T3NS structures, but not for the MPS. The simulations using the MPS cannot achieve an error below 10^{-2} at all. Notably, the TTNS also requires similar or fewer resources, both in terms of memory and runtime, compared to the MPS to achieve the same error. This supports that long-range interactions cause problems for less optimized structures, thereby demonstrating that TTN can provide an advantage over the simpler tensor train structure. When examining methods other than the Zip-Up method, we observe them performing within a similar range. However, the SRC performs slightly worse, requiring more memory and runtime to achieve a desired error. For the other three methods, there is no relevant difference in performance when considering the memory requirement. Surprisingly, the performance regarding runtime is the opposite of our initial expectation. The contraction and truncation algorithm performs best, followed by the DM-based method and then our CBC method. This is likely due to the very low bond dimension of the TTNO, which represents the quantum circuit.

V. CONCLUSION

We found that our newly introduced CBC method, which applies a TTNO to a TTNS, performs similarly to current state-of-the-art methods, such as SRC and DM. We also found that the correct choice of method can be impacted significantly by the relative bond dimension of TTNO to TTNS. In all our numerical studies, the CBC method consistently performed among the best. Another advantage of our method over the SRC is the simpler implementation of an automatically adaptive bond dimension by setting a tolerance for the SVD. The flip side of this is that the SRC only requires contractions and QR decompositions, which allows a much greater performance boost when running the simulations on GPUs [72]. Additionally, our results support the utility of more complicated TTN structures adapted to the problem at hand, improving once more the classical methods to simulate quantum systems. We can also conclude that the Zip-Up method performs significantly worse than the CBC



(a) In this structure, groups of sites with high interaction are placed on chains, and only the site interacting with the remaining system is connected to the remaining tensor network. The three sites that facilitate interaction between the highly interacting regions are placed on intermediate tensors attached to the root.

(b) In this structure, groups of sites that interact strongly are represented by tensors that are close to each other. However, the tensors are not directly connected. On the other hand, the three sites facilitating the interaction between these groups are also not directly attached to the root, but represented by a leaf tensor.

FIG. 7: The two different T3NS structures used in the circuit simulation.

and SRC methods in every aspect and should therefore no longer be considered state-of-the-art. Additionally, we found that the DM bases compression method, while useful for MPS, is unsuited for general T3NS.

ACKNOWLEDGMENTS

The research is part of the Munich Quantum Valley, which is supported by the Bavarian state government

with funds from the Hightech Agenda Bayern Plus. The visit of RM to the California Institute of Technology, during which part of the research for this work was carried out, was additionally supported by the Internationalisierungsförderung of the TUM Graduate School. Shuo Sun acknowledges funding by the BMW Group.

[1] Y.-Y. Shi, L.-M. Duan, and G. Vidal, Classical simulation of quantum many-body systems with a tree tensor network, *Phys. Rev. A* **74**, [10.1103/PhysRevA.74.022320](https://doi.org/10.1103/PhysRevA.74.022320) (2006).

[2] P. Silvi, F. Tschirsich, M. Gerster, J. Jünemann, D. Jaschke, M. Rizzi, and S. Montangero, The tensor networks anthology: Simulation techniques for many-body quantum lattice systems, *SciPost Physics Lecture Notes* [10.21468/SciPostPhysLectNotes.8](https://doi.org/10.21468/SciPostPhysLectNotes.8) (2019).

[3] H. R. Larsson, Computing vibrational eigenstates with tree tensor network states (TTNS), *J. Chem. Phys.* **151**, [10.1063/1.5130390](https://doi.org/10.1063/1.5130390) (2019).

[4] H. R. Larsson, A tensor network view of multilayer multi-configuration time-dependent Hartree methods, *Molecular Physics* **122**, [10.1080/00268976.2024.2306881](https://doi.org/10.1080/00268976.2024.2306881) (2024).

[5] H. R. Larsson, Benchmarking vibrational spectra: 5000 accurate eigenstates of acetonitrile using tree tensor network states, *The Journal of Physical Chemistry Letters* **16**, [10.1021/acs.jpclett.5c00782](https://doi.org/10.1021/acs.jpclett.5c00782) (2025).

[6] W. Li, J. von Delft, and T. Xiang, Efficient simulation of infinite tree tensor network states on the Bethe lattice, *Phys. Rev. B* **86**, [10.1103/PhysRevB.86.195137](https://doi.org/10.1103/PhysRevB.86.195137) (2012).

[7] N. Nakatani and G. K.-L. Chan, Efficient tree tensor network states (TTNS) for quantum chemistry: Generalizations of the density matrix renormalization group algorithm, *J. Chem. Phys.* **138**, [10.1063/1.4798639](https://doi.org/10.1063/1.4798639) (2013).

[8] D. Sulz, C. Lubich, G. Ceruti, I. Lesanovsky, and F. Carollo, Numerical simulation of long-range open quantum many-body dynamics with tree tensor networks, *Phys. Rev. A* **109**, [10.1103/PhysRevA.109.022420](https://doi.org/10.1103/PhysRevA.109.022420) (2024).

[9] P. Seitz, I. Medina, E. Cruz, Q. Huang, and C. B. Mendl, Simulating quantum circuits using tree tensor networks, *Quantum* **7**, [10.22331/q-2023-03-30-964](https://doi.org/10.22331/q-2023-03-30-964) (2023).

[10] A. Dubey, Z. Zeybek, and P. Schmelcher, Simulating quantum circuits with tree tensor networks using density-matrix renormalization group algorithm, *Phys. Rev. B*

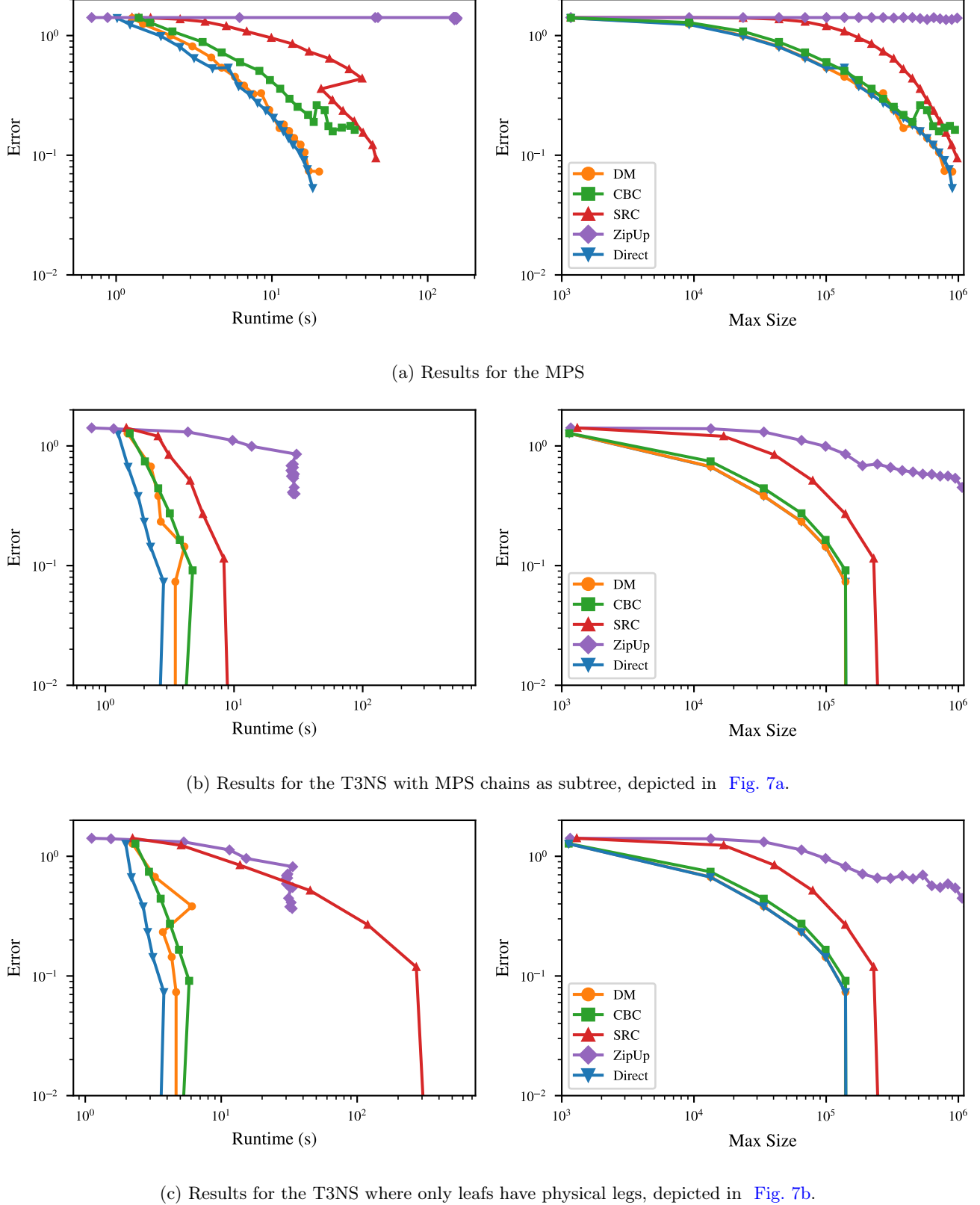


FIG. 8: Runtime (left) and maximum tensor network size during the run (right) plotted against the error of the performed circuit simulation for three different tree structures. Every point is a different maximally allowed bond dimension.

112, [10.1103/64hd-q4z5](https://doi.org/10.1103/64hd-q4z5) (2025).

[11] V. Murg, F. Verstraete, O. Legeza, and R. M. Noack, Simulating strongly correlated quantum systems with tree tensor networks, *Phys. Rev. B* **82**, [10.1103/PhysRevB.82.205105](https://doi.org/10.1103/PhysRevB.82.205105) (2010).

[12] Y. Ke, Tree tensor network state approach for solving hierarchical equations of motion, *J. Chem. Phys.* **158**, [10.1063/5.0153870](https://doi.org/10.1063/5.0153870) (2023).

[13] Y. Ke and J. Assan, Harnessing multi-mode optical structure for chemical reactivity, *J. Chem. Phys.* **163**, [10.1063/5.0292193](https://doi.org/10.1063/5.0292193) (2025).

[14] Y. Ke, Stochastic resonance in vibrational polariton chemistry, *J. Chem. Phys.* **162**, [10.1063/5.0248419](https://doi.org/10.1063/5.0248419) (2025).

[15] J. Schuhmacher, M. Ballarin, A. Baiardi, G. Magnifico, F. Tacchino, S. Montangero, and I. Tavernelli, Hybrid tree tensor networks for quantum simulation, *PRX Quantum* **6**, [10.1103/PRXQuantum.6.010320](https://doi.org/10.1103/PRXQuantum.6.010320) (2025).

[16] S. Sun, R. M. Milbradt, S. Knecht, C. Kumar, and C. B. Mendl, Tree tensor networks methods for efficient calculation of molecular vibrational spectra, *arXiv* [10.48550/ARXIV.2512.15875](https://arxiv.org/abs/10.48550/ARXIV.2512.15875) (2025).

[17] M. Rakhuba and I. Oseledets, Calculating vibrational spectra of molecules using tensor train decomposition, *J. Chem. Phys.* **145**, [10.1063/1.4962420](https://doi.org/10.1063/1.4962420) (2016).

[18] A. Baiardi, C. J. Stein, V. Barone, and M. Reiher, Optimization of highly excited matrix product states with an application to vibrational spectroscopy, *J. Chem. Phys.* **150**, [10.1063/1.5068747](https://doi.org/10.1063/1.5068747) (2019).

[19] Y. Wang, M. Luo, M. Reumann, and C. B. Mendl, Enhanced Krylov methods for molecular Hamiltonians: Reduced memory cost and complexity scaling via tensor hypercontraction, *J. Chem. Theory Comput.* **21**, [10.1021/acs.jctc.5c00525](https://doi.org/10.1021/acs.jctc.5c00525) (2025).

[20] Y. Wang, Z. Yang, X. Wu, and C. B. Mendl, An optimally accurate Lanczos algorithm in the matrix product state representation, *arXiv* [10.48550/ARXIV.2504.21786](https://arxiv.org/abs/10.48550/ARXIV.2504.21786) (2025).

[21] A. Dektor, P. DelMastro, E. Ye, R. Van Beeumen, and C. Yang, Inexact subspace projection methods for low-rank tensor eigenvalue problems, *arXiv* [10.48550/ARXIV.2502.19578](https://arxiv.org/abs/10.48550/ARXIV.2502.19578) (2025).

[22] F. Verstraete and J. I. Cirac, Renormalization algorithms for quantum-many body systems in two and higher dimensions, *arXiv* [10.48550/arXiv.cond-mat/0407066](https://arxiv.org/abs/10.48550/arXiv.cond-mat/0407066) (2004).

[23] M. Lubasch, J. I. Cirac, and M.-C. Bañuls, Unifying projected entangled pair state contractions, *New J. Phys.* **16**, [10.1088/1367-2630/16/3/033014](https://doi.org/10.1088/1367-2630/16/3/033014) (2014).

[24] M. P. Zaletel, R. S. K. Mong, C. Karrasch, J. E. Moore, and F. Pollmann, Time-evolving a matrix product state with long-ranged interactions, *Phys. Rev. B* **91**, [10.1103/PhysRevB.91.165112](https://doi.org/10.1103/PhysRevB.91.165112) (2015).

[25] S. Paekel, T. Köhler, A. Swoboda, S. R. Manmana, U. Schollwöck, and C. Hubig, Time-evolution methods for matrix-product states, *Ann. Physics* **411**, [10.1016/j.aop.2019.167998](https://doi.org/10.1016/j.aop.2019.167998) (2019).

[26] L. B. Gaggioli and J. Mareček, Time evolution of controlled many-body quantum systems with matrix product operators, *arXiv* [10.48550/arXiv.2509.07228](https://arxiv.org/abs/10.48550/arXiv.2509.07228) (2025).

[27] P. E. Dargel, A. Wöllert, A. Honecker, I. P. McCulloch, U. Schollwöck, and T. Pruschke, Lanczos algorithm with matrix product states for dynamical correlation functions, *Phys. Rev. B* **85**, [10.1103/PhysRevB.85.205119](https://doi.org/10.1103/PhysRevB.85.205119) (2012).

[28] M. L. Wall and L. D. Carr, Out-of-equilibrium dynamics with matrix product states, *New J. Phys.* **14**, [10.1088/1367-2630/14/12/125015](https://doi.org/10.1088/1367-2630/14/12/125015) (2012).

[29] M. Yang and S. R. White, Time-dependent variational principle with ancillary Krylov subspace, *Phys. Rev. B* **102**, [10.1103/PhysRevB.102.094315](https://doi.org/10.1103/PhysRevB.102.094315) (2020).

[30] A. Strathearn, P. Kirton, D. Kilda, J. Keeling, and B. W. Lovett, Efficient non-Markovian quantum dynamics using time-evolving matrix product operators, *Nature Communications* **9**, [10.1038/s41467-018-05617-3](https://doi.org/10.1038/s41467-018-05617-3) (2018).

[31] M. Richter and S. Hughes, Enhanced TEMPO algorithm for quantum path integrals with off-diagonal system-bath coupling: Applications to photonic quantum networks, *Phys. Rev. Lett.* **128**, [10.1103/PhysRevLett.128.167403](https://doi.org/10.1103/PhysRevLett.128.167403) (2022).

[32] A. Bose and P. L. Walters, A tensor network representation of path integrals: Implementation and analysis, *arXiv* (2023).

[33] E. Ye and G. K.-L. Chan, Constructing tensor network influence functionals for general quantum dynamics, *J. Chem. Phys.* **155**, [10.1063/5.0047260](https://doi.org/10.1063/5.0047260) (2021).

[34] J. Chen, E. Stoudenmire, and S. R. White, Quantum Fourier transform has small entanglement, *PRX Quantum* **4**, [10.1103/PRXQuantum.4.040318](https://doi.org/10.1103/PRXQuantum.4.040318) (2023).

[35] P. Gelfß, S. Klus, S. Knebel, Z. Shakibaei, and S. Pokutta, Low-rank tensor decompositions of quantum circuits, *arXiv* [10.48550/arXiv.2205.09882](https://arxiv.org/abs/10.48550/arXiv.2205.09882) (2023).

[36] U. Schollwöck, The density-matrix renormalization group in the age of matrix product states, *Ann. Physics* January 2011 Special Issue, **326**, [10.1016/j.aop.2010.09.012](https://doi.org/10.1016/j.aop.2010.09.012) (2011).

[37] J. C. Bridgeman and C. T. Chubb, Hand-waving and interpretive dance: An introductory course on tensor networks, *J. Phys. A: Math. Theor.* **50**, [10.1088/1751-8121/aa6dc3](https://doi.org/10.1088/1751-8121/aa6dc3) (2017).

[38] G. Evenbly, A practical guide to the numerical implementation of tensor networks I: Contractions, decompositions and gauge freedom, *arXiv* (2022).

[39] R. Orús, Tensor networks for complex quantum systems, *Nature Reviews Physics* **1**, [10.1038/s42254-019-0086-7](https://doi.org/10.1038/s42254-019-0086-7) (2019).

[40] J. I. Cirac, D. Pérez-García, N. Schuch, and F. Verstraete, Matrix product states and projected entangled pair states: Concepts, symmetries, theorems, *Rev. Mod. Phys.* **93**, [10.1103/RevModPhys.93.045003](https://doi.org/10.1103/RevModPhys.93.045003) (2021).

[41] M. C. Bañuls, Tensor network algorithms: A route map, *Annu. Rev. Condens. Matter Phys.* **14**, [10.1146/annurev-conmatphys-040721-022705](https://doi.org/10.1146/annurev-conmatphys-040721-022705) (2023).

[42] I. V. Oseledets, Tensor-train decomposition, *SIAM J. Sci. Comp.* **33**, [10.1137/090752286](https://doi.org/10.1137/090752286) (2011).

[43] K. Gunst, F. Verstraete, S. Wouters, O. Legeza, and D. Van Neck, T3NS: Three-legged tree tensor network states, *J. Chem. Theory Comput.* **14**, [1549](https://doi.org/10.1021/acs.jctc.8b00014) (2018).

[44] L. Tagliacozzo, G. Evenbly, and G. Vidal, Simulation of two-dimensional quantum systems using a tree tensor network that exploits the entropic area law, *Phys. Rev. B* **80**, [10.1103/PhysRevB.80.235127](https://doi.org/10.1103/PhysRevB.80.235127) (2009).

[45] S. Cheng, L. Wang, T. Xiang, and P. Zhang, Tree tensor networks for generative modeling, *Phys. Rev. B* **99**, [10.1103/PhysRevB.99.155131](https://doi.org/10.1103/PhysRevB.99.155131) (2019).

[46] W. Krinitzin, N. Tausendpfund, M. Heyl, M. Rizzi, and M. Schmitt, Time evolution of the quantum Ising model in two dimensions using tree tensor networks, *Phys. Rev.*

B **112**, [10.1103/kj16-sqcm](https://doi.org/10.1103/kj16-sqcm) (2025).

[47] K. Gunst, F. Verstraete, and D. Van Neck, Three-legged tree tensor networks with $SU(2)$ and molecular point group symmetry, *J. Chem. Theory Comput.* **15**, [10.1021/acs.jctc.9b00071](https://doi.org/10.1021/acs.jctc.9b00071) (2019).

[48] P. Silvi, V. Giovannetti, S. Montangero, M. Rizzi, J. I. Cirac, and R. Fazio, Homogeneous binary trees as ground states of quantum critical Hamiltonians, *Phys. Rev. A* **81**, [10.1103/PhysRevA.81.062335](https://doi.org/10.1103/PhysRevA.81.062335) (2010).

[49] G. Magnifico, T. Felser, P. Silvi, and S. Montangero, Lattice quantum electrodynamics in (3+1)-dimensions at finite density with tensor networks, *Nature Comm.* **12**, [10.1038/s41467-021-23646-3](https://doi.org/10.1038/s41467-021-23646-3) (2021).

[50] G. Ceruti, C. Lubich, and H. Walach, Time integration of tree tensor networks, *SIAM J. Numer. Anal.* **59**, [10.1137/20M1321838](https://doi.org/10.1137/20M1321838) (2021).

[51] K. Okunishi, H. Ueda, and T. Nishino, Entanglement bipartitioning and tree tensor networks, *Prog. Theor. Exp. Phys.* **2023**, [10.1093/ptep/ptad018](https://doi.org/10.1093/ptep/ptad018) (2023).

[52] G. Ceruti, C. Lubich, and D. Sulz, Rank-adaptive time integration of tree tensor networks, *SIAM J. Numer. Anal.* **61**, [10.1137/22M1473790](https://doi.org/10.1137/22M1473790) (2023).

[53] F. Fröwis, V. Nebendahl, and W. Dür, Tensor operators: Constructions and applications for long-range interaction systems, *Phys. Rev. A* **81**, [10.1103/PhysRevA.81.062337](https://doi.org/10.1103/PhysRevA.81.062337) (2010).

[54] R. M. Milbradt, Q. Huang, and C. B. Mendl, State diagrams to determine tree tensor network operators, *SciPost Phys. Core* **7**, [10.21468/scipostphyscore.7.2.036](https://doi.org/10.21468/scipostphyscore.7.2.036) (2024).

[55] D. Bauernfeind and M. Aichhorn, Time dependent variational principle for tree tensor networks, *SciPost Phys.* **8**, [024](https://doi.org/10.21468/scipostphys.8.024) (2020).

[56] J. Ren, W. Li, T. Jiang, Y. Wang, and Z. Shuai, Time-dependent density matrix renormalization group method for quantum dynamics in complex systems, *Wiley Interdiscip. Rev. Comput. Mol. Sci.* **12**, [e1614](https://doi.org/10.1002/wic.1614) (2022).

[57] G. Ceruti, J. Kusch, C. Lubich, and D. Sulz, A parallel basis update and Galerkin integrator for tree tensor networks, [arXiv 10.48550/arXiv.2412.00858](https://arxiv.org/abs/10.48550/arXiv.2412.00858) (2024).

[58] W. Li, J. Ren, H. Yang, H. Wang, and Z. Shuai, Optimal tree tensor network operators for tensor network simulations: Applications to open quantum systems, *J. Chem. Phys.* **161** (2024).

[59] H. Çakir, R. M. Milbradt, and C. B. Mendl, Optimal symbolic construction of matrix product operators and tree tensor network operators, *Phys. Rev. B* **112**, [10.1103/8993-8xn5](https://doi.org/10.1103/8993-8xn5) (2025).

[60] The DMC algorithm has no first paper associated with it. However, it is included in the ITensor tensor network library [73, 74] and pedagogically explained in [75].

[61] L. Ma, M. Fishman, M. Stoudenmire, and E. Solomonik, Approximate contraction of arbitrary tensor networks with a flexible and efficient density matrix algorithm, *Quantum* **8**, [10.22331/q-2024-12-27-1580](https://doi.org/10.22331/q-2024-12-27-1580) (2024).

[62] H. Al Daas, G. Ballard, P. Cazeaux, E. Hallman, A. Międlar, M. Pasha, T. W. Reid, and A. K. Saibaba, Randomized algorithms for rounding in the tensor-train format, *SIAM J. Sci. Comp.* **45**, [10.1137/21M1451191](https://doi.org/10.1137/21M1451191) (2023).

[63] C. Camañ, E. N. Epperly, and J. A. Tropp, Successive randomized compression: A randomized algorithm for the compressed MPO-MPS product, [arXiv 10.48550/arXiv.2504.06475](https://arxiv.org/abs/10.48550/arXiv.2504.06475) (2025).

[64] E. M. Stoudenmire and S. R. White, Minimally entangled typical thermal state algorithms, *New J. Phys.* **12**, [10.1088/1367-2630/12/5/055026](https://doi.org/10.1088/1367-2630/12/5/055026) (2010).

[65] TensorNetwork.org contributors, TensorNetwork.org: MPO-MPS multiplication: Zip-Up algorithm (2021).

[66] N. Halko, P. G. Martinsson, and J. A. Tropp, Finding structure with randomness: Probabilistic algorithms for constructing approximate matrix decompositions, *SIAM Rev.* **53**, [10.1137/090771806](https://doi.org/10.1137/090771806) (2011).

[67] R. Murray, J. Demmel, M. W. Mahoney, N. B. Erichson, M. Melnichenko, O. A. Malik, L. Grigori, P. Luszczek, M. Dereziński, M. E. Lopes, T. Liang, H. Luo, and J. Dongarra, Randomized numerical linear algebra: A perspective on the field with an eye to software, [arXiv 10.48550/arXiv.2302.11474](https://arxiv.org/abs/10.48550/arXiv.2302.11474) (2023).

[68] R. M. Milbradt, Q. Huang, and C. B. Mendl, PyTreeNet: A python library for easy utilisation of tree tensor networks, [arXiv 10.48550/arXiv.2407.13249](https://arxiv.org/abs/10.48550/arXiv.2407.13249) (2024).

[69] R. M. Milbradt, H. Çakir, Q. Huang, and S. Sun, PyTreeNet repository, <https://github.com/Drachier/PyTreeNet> (2025).

[70] J. Jiang, J. Chen, N. Schuch, and D. Hangleiter, Positive bias makes tensor-network contraction tractable, in *Proceedings of the 57th Annual ACM Symposium on Theory of Computing* (Prague Czechia, 2025).

[71] D. Bauernfeind, M. Zingl, R. Triebel, M. Aichhorn, and H. G. Evertz, Fork tensor-product states: Efficient multiorbital real-time DMFT solver, *Phys. Rev. X* **7**, [10.1103/PhysRevX.7.031013](https://doi.org/10.1103/PhysRevX.7.031013) (2017).

[72] J. Unfried, J. Hauschild, and F. Pollmann, Fast time evolution of matrix product states using the QR decomposition, *Phys. Rev. B* **107**, [10.1103/PhysRevB.107.155133](https://doi.org/10.1103/PhysRevB.107.155133) (2023).

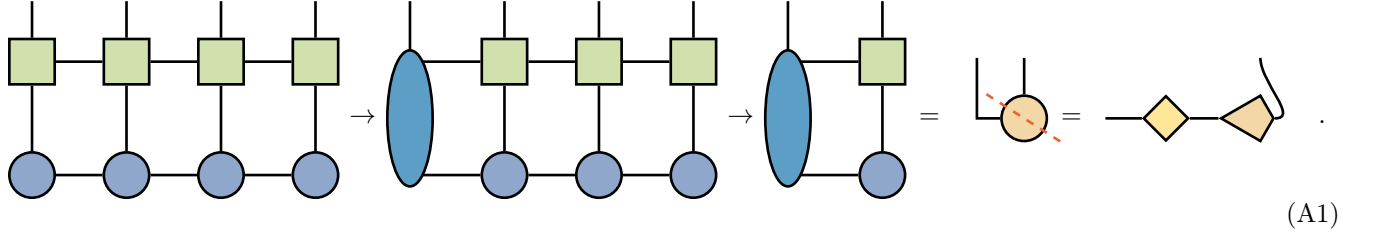
[73] M. Fishman, S. R. White, and E. M. Stoudenmire, The ITensor software library for tensor network calculations, *SciPost Phys. Codebases* **4** (2022).

[74] M. Fishman, S. R. White, and E. M. Stoudenmire, Codebase release 0.3 for ITensor, *SciPost Phys. Codebases* **4** (2022).

[75] TensorNetwork.org contributors, TensorNetwork.org: MPO-MPS multiplication: Density matrix algorithm (2021).

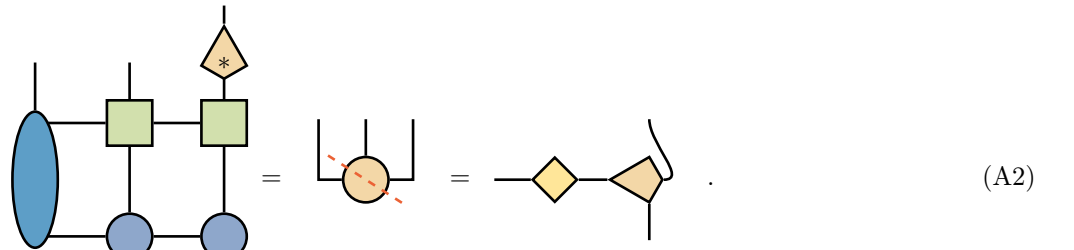
Appendix A: Illustration of CBC for an MPS

This appendix illustrates the various steps of the CBC for a length-4 MPS. The first step is the construction of the left subtree tensors \mathcal{L} via repeated contraction and truncation until we reach the right-most site.



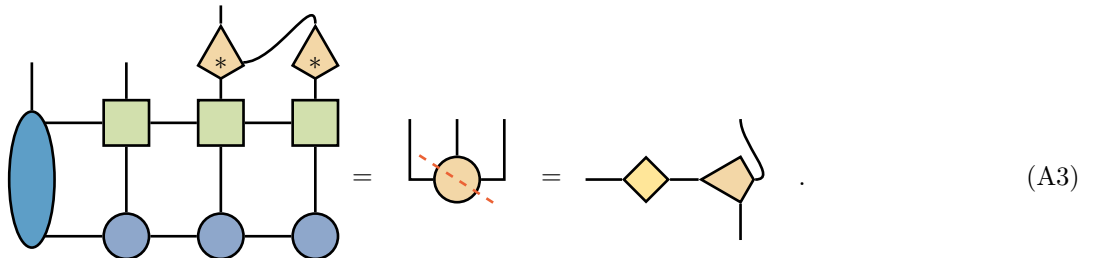
In the end, we obtain a tensor of dimensions \bar{D} and d , shown in orange in the previous equation. It is decomposed via the QR decomposition to yield an isometric tensor, which will be the rightmost tensor in the new MPS, while the non-isometric matrix is no longer needed.

We then proceed to one site to the left. Here, we reuse the left subtree tensor obtained in the previous step, and we project the right-most site to the desired bond dimension, yielding



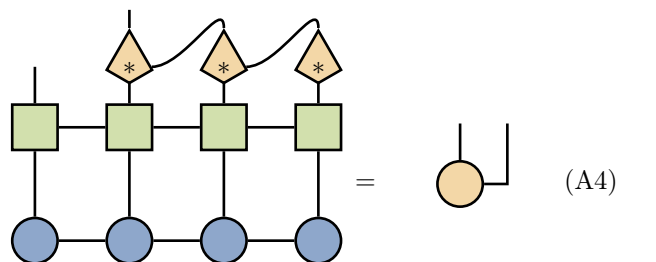
Where once more the final isometric tensor is the site's

tensor in the new MPS. Moving to the second-to-last site, we again proceed similarly



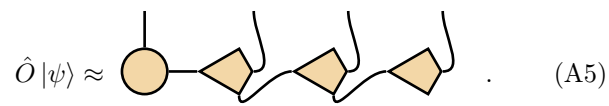
Note that here the projection tensor of the rightmost site is contracted with the next projection tensor. Here, it is reasonable to reuse a partial contraction result from the previous site to avoid unnecessary computations. This reused part is exactly what we defined as the right subtree tensors earlier. If the MPS were longer, the above steps would be repeated until the last site is reached. For the

last site, we merely contract



to obtain the tensor of the leftmost site. In total, the MPS resulting from the application of the MPO will then

have the form

$$\hat{O} |\psi\rangle \approx \text{Diagram} \quad . \quad (\text{A5})$$


The diagram consists of a vertical line ending in a circle, representing an incoming particle. This line connects to a sequence of three vertices, each represented by a triangle pointing to the right. Each vertex is connected to a wavy line that curves upwards and to the right, representing an outgoing particle. The entire sequence of vertices and wavy lines is enclosed in a bracket on the right side, indicating a sum over different configurations.